Impact of nuclear dynamics on interatomic Coulombic decay in a He dimer

Nicolas Sisourat,[1,*] Nikolai V. Kryzhevoi,[1] Přemysl Kolorenč,[2] Simona Scheit,[3] and Lorenz S. Cederbaum[1]

[1]*Theoretische Chemie, Universität Heidelberg, Im Neuenheimer Feld 229, D-69120 Heidelberg, Germany*

[2]*Faculty of Mathematics and Physics, Institute of Theoretical Physics, Charles University in Prague, V Holešovičkách 2, CZ-18000 Prague, Czech Republic*

[3]*Department of Basic Science, Graduate School of Arts and Sciences, University of Tokyo, Komaba, 153-8902 Tokyo, Japan*

(Received 13 August 2010; published 3 November 2010)

After simultaneous ionization and excitation of one helium atom within the giant weakly bound helium dimer, the excited ion can relax via interatomic Coulombic decay (ICD) and the excess energy is transferred to ionize the neighboring helium atom. We showed [Sisourat *et al.* Nature Phys. **6**, 508 (2010)] that the distributions of the kinetic energy released by the two ions reflect the nodal structures of the ICD-involved vibrational wave functions. We also demonstrated that energy transfer via ICD between the two helium atoms can take place over more than 14 Å. We report here a more detailed analysis of the ICD process and of the impact of the nuclear dynamics on the electronic decay. Nonadiabatic effects during the ICD process and the accuracy of the potential energy curve of helium dimer and of the computed decay rates are also investigated.

DOI: 10.1103/PhysRevA.82.053401 PACS number(s): 33.80.Eh, 36.40.−c

I. INTRODUCTION

Excited states of isolated atoms or molecules have, in general, two possibilities to decay to a stable state: by emitting a photon (radiative decay) or by emitting an electron (Auger decay). One should mention, however, that in the case of molecules, vibrational relaxation is also conceivable. Isolated inner-valence ionized systems usually cannot decay nonradiatively, i.e., by emitting a secondary electron, since the energy of the inner-valence vacancy state lies below the double ionization threshold and thus the process is energetically forbidden. The situation changes substantially if the inner-valence ionized system is embedded in an environment like in a cluster, for instance. In this case, an electronic relaxation mechanism called interatomic (or intermolecular) Coulombic decay (ICD) becomes possible [1]: After inner-valence ionization of a particular subunit of the cluster, the vacancy is refilled by an outer-valence electron of the same cluster subunit and the energy gained in this process is transferred to another cluster subunit, where a secondary electron is emitted from the outer-valence shell. The final state is thus characterized by two outer-valence vacancies, each on a different cluster subunit. Due to repulsion between the two positive charges produced after the ICD process, the cluster may undergo a Coulomb explosion and break into two or more fragments. ICD was theoretically predicted in 1997 and, since then, observed experimentally in van der Waals clusters [2–6] as well as in hydrogen bonded systems [7–9].

Another ICD-like process was observed after simultaneous ionization and excitation of one atom in neon dimer [10]. Recently, it was observed in the giant helium dimer [11]. After simultaneous ionization and excitation of one helium atom in the dimer, the resulting excited helium ion relaxes via ICD to $He^+(1s)$ and the neutral helium is ionized. The two $He^+(1s)$ then undergo a Coulomb explosion and fly apart. In short:

$$\begin{aligned} \text{He–He} &\xrightarrow{h\nu} [\text{He}^{+*}\text{–He}] + e^-_{\text{ph}} \\ &\xrightarrow{\text{ICD}} [\text{He}^+ + \text{He}^+ + e^-_{\text{ICD}}] + e^-_{\text{ph}}. \end{aligned} \quad (1)$$

The ICD process was observed unambiguously by measuring in coincidence the kinetic energy of the emitted ICD electron and that of the two ions [11]. In a previous article (Ref. [12]), we showed that the two helium atoms can exchange energy over huge distances, up to 14 Å. It was also demonstrated that the total kinetic energy release (KER) spectrum exhibits structures which are images of the vibrational wave functions participating in the ICD process. We report here a detailed analysis of the ICD process in helium dimer and of the impact of the nuclear dynamics on the electronic decay. In the next section, we present the *ab initio* methods we used to compute the KER distributions. Then, the results of the computations are shown and discussed. Finally, we investigate the effects of nonadiabatic coupling and the impact of varying the decay rates on the ICD process.

II. METHODS

We computed fully *ab initio* the distributions of the kinetic energy released by the two helium ions after ICD. In order to compute these distributions, one needs the potential energy curves (PECs) and the corresponding decay rates of the involved electronic states as a function of the interatomic distance R. The details of computations of PECs and decay rates are given in Ref. [13]. We give here a short overview of the methods: the PECs were computed using the full configuration interaction (FCI) method with a 6-ζ quality basis set on each helium atom. The PEC of the neutral helium dimer was initially taken from Tang *et al.* [14]. Recently, a new PEC for this state was published in Ref. [15]. We compare here the total KER spectrum obtained with each of these PECs. The decay rates for each state were obtained by the symmetry-adapted Fano-Green's functions Stieltjes imaging technique [16,17]. We summarize the results of these computations in Fig. 1 and in Fig. 2.

In order to investigate the impact of the nuclear dynamics on the decay process, we computed the KER spectrum for each ICD channel as function of time. The KER spectrum is written in terms of eigenvectors and eigenvalues [18] of the nuclear Hamiltonian of the neutral helium dimer (He-He), the initial (He^{+*}-He), and the final (He^+-He^+) electronic states.

*nicolas.sisourat@pci.uni-heidelberg.de

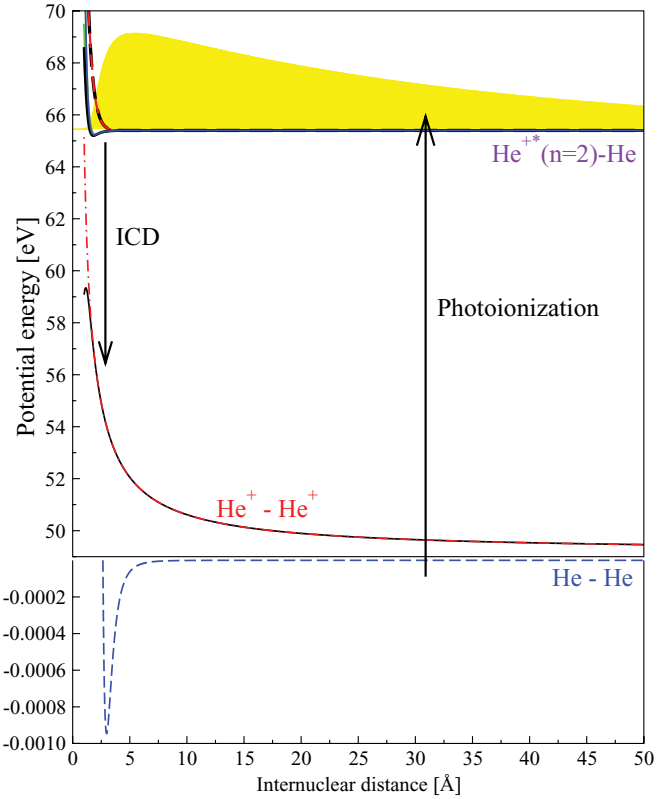

FIG. 1. (Color online) Potential energy curves for He-He (dashed blue line), He^+-He^+ (dashed-dotted red line and full black line), and $He^+(n=2)$-He (color lines, see Fig. 2) states. The nuclear wave function of the ground state of the dimer is shown in yellow. After photoionization of a helium atom in the dimer, the system is left in one of the $He^+(n=2)$-He states. The excited He^+ relaxes by transferring its energy via ICD to ionize the neighboring helium atom which emits the ICD electron. The system ends in dissociative He^+-He^+ states.

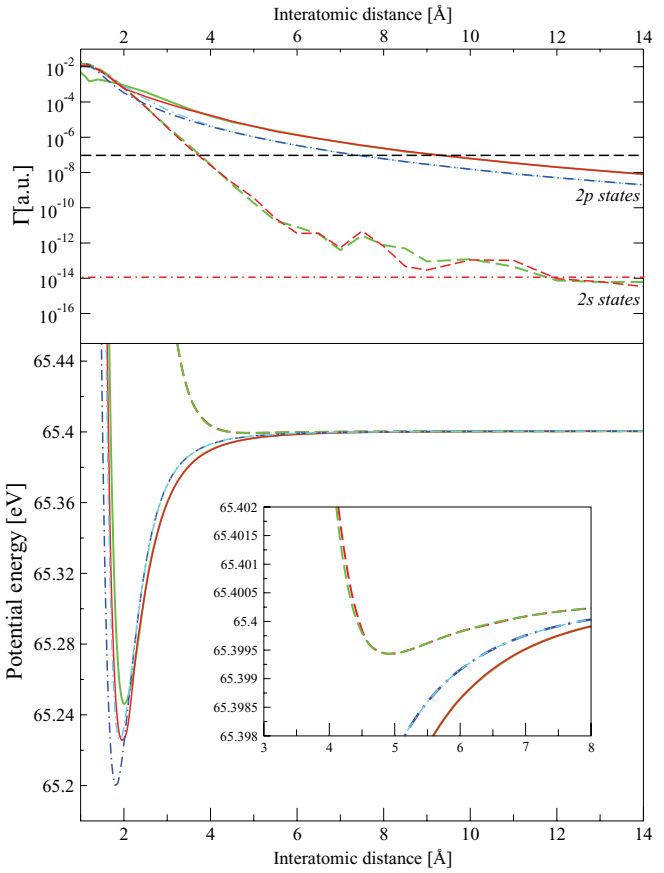

FIG. 2. (Color online) *Ab initio* data relevant for ICD in He_2. Top panel: ICD rates (in atomic units) for the decaying $He^+(n=2)$-He states: $^2\Sigma_u^+$:$2p_z$ (red (dark gray) line), $^2\Sigma_g^+$:$2p_z$ (green (light gray) line), $^2\Pi_u$:$2p_{x,y}$ (dashed-dotted cyan (light gray) line), $^2\Pi_g$:$2p_{x,y}$ (dashed-dotted blue (dark gray) line), $^2\Sigma_u^+$:$2s$ (dashed red (dark gray) line) and $^2\Sigma_g^+$:$2s$ (dashed green (light gray) line). The horizontal lines in the top panel indicate the values of the radiative decay rates for $He^+(2s)$ (dashed-dotted red line) and for $He^+(2p)$ (dashed black line). Lower panels: Potential energy curves of the $He^+(n=2)$-He states decaying by ICD (same color notation as in top panel).

Assuming broadband excitation, the KER spectrum at time t is given by

$$\sigma(E_f,t) = \int dE_e |c(E_e,E_f,t)|^2 \tag{2}$$

with

$$c(E_e,E_f,t) = \sum_{j=1}^{n_d} \frac{\langle F_f|\hat{W}|D_j\rangle\langle D_j|I\rangle}{E_e + E_f - \epsilon_j + i\Gamma_j/2} \times (1 - e^{-i[E_e+E_f-(\epsilon_j+i\Gamma_j/2)]t}), \tag{3}$$

where E_e, E_f (= KER), and $\epsilon_j + i\Gamma_j/2$ are the energy of the ICD electron, of the final state $|F_f\rangle$, and of the decaying state $|D_j\rangle$, respectively. The states $|I\rangle$ and $|F_f\rangle$ are the nuclear eigenstates of the neutral He-He and the final He^+-He^+ electronic states, respectively. The states $|D_j\rangle$ are the right-hand eigenstates of the complex Hamiltonian $\hat{H}_d$ of the electronic decaying state. The number n_d of decaying nuclear eigenstates was chosen to ensure convergence of the results. The operator $\hat{W}$ is equal to $\sqrt{2\pi\gamma_D}$, where γ_D is the partial ICD rate. The Hamiltonian $\hat{H}_d$ is written in the local approximation [19] as

$$\hat{H}_d = \hat{T}_N + V_D(R) - i\frac{\Gamma_D(R)}{2}, \tag{4}$$

where $\hat{T}_N$ is the kinetic energy operator and $V_D(R)$ and $\Gamma_D(R)$ are the corresponding PEC and the total decay rate, respectively. Note that the total decay rate is the sum of the ICD rate and the radiative decay rate.

The equations presented above are valid in the adiabatic approximation, i.e., the electronic states can be considered independent of each other. However, when two molecular electronic states with the same symmetry are close in energy to each other the commonly used adiabatic representation (Born-Oppenheimer approximation) breaks down. It is discussed in Ref. [20] how to incorporate the nonadiabatic coupling into the formalism of decaying states. A diabatic representation which couples the molecular states is then favorable. Therefore, instead of the Hamiltonian $\hat{H}_d$ given in Eq. (4), a more general Hamiltonian must be used:

$$H_D = \begin{pmatrix} H_D^i & C^{ij} \\ C^{ij} & H_D^j \end{pmatrix}, \tag{5}$$

where H_D^i and H_D^j are the nuclear Hamiltonians of the uncoupled electronic states and C^{ij} is their coupling in the diabatic representation, respectively. Details of the computations of the nonadiabatic coupling are given later on in this article.

The computation of the eigenvectors and eigenvalues of the different electronic states was done using a grid finite difference method and the inverse iteration method [21]. The helium dimer in its electronic ground state possesses only one vibrational bound state which has an average internuclear distance of around 52 Å. A large grid of 8000 grid points which spans over 425 Å was used to describe correctly this vibrational state. To represent the vibrational decaying $|D_j\rangle$ states, we used a smaller 80 Å grid of 4000 grid points. The ten first low-lying dissociative states were computed as well. The final $|F_f\rangle$ states were computed on a 50 Å grid of 8000 grid points. We made sure that the computed cross sections are converged with respect to the size and the number of points of the different grids.

III. RESULTS

We consider in the present report a photon energy range in which only $He^+(n = 2)$ can be reached in the photoionization process. Therefore, only molecular states of He_2^+ which correspond to $He^+(n = 2)$-He states at infinite internuclear distance have to be taken into account for describing the ICD process. The PECs are shown in Figs. 1 and 2. We label the electronic states by their configuration term and the atomic state of the excited He^+ in the asymptotic limit ($R \to \infty$). Two kinds of PECs are identified. Those of the first kind are related to the so-called *2p states*, denoted $^2\Sigma_g^+$:$2p_z$, $^2\Sigma_u^+$:$2p_z$, $^2\Pi_u$:$2p_{x,y}$, and $^2\Pi_g$:$2p_{x,y}$, which exhibit minima around 2 Å. The electronic states of the second kind are related to the so-called *2s states*, denoted $^2\Sigma_g^+$:$2s$,$^2\Sigma_u^+$:$2s$, which possess shallower minima at around 5 Å. Each of these electronic states can decay to He^+-He^+ singlet and triplet final states ($^1\Sigma_g^+$ and $^3\Sigma_u^+$). Note that nonadiabatic coupling between $^2\Sigma_g^+$:$2p_z$ and $^2\Sigma_g^+$:$2s$ states on one hand and $^2\Sigma_u^+$:$2p_z$ and $^2\Sigma_u^+$:$2s$ states on the other hand occurs. Therefore, the states within each pair have to be considered together. We discuss the effect of nonadiabatic coupling on the ICD process later. The corresponding ICD rates as a function of R are depicted in the top panel of Fig. 2. As seen in the figure, the ICD rates strongly depend on R; the shorter the distance between the atoms is, the faster is the ICD. The ICD rates of the *2p* and *2s states* must be compared to their corresponding radiative decay rates. The radiative decay is an atomic property and the extremely weak He-He interaction within the dimer has little influence on it. Therefore, the radiative decay rate is assumed to be constant over the relevant internuclear distances. According to the atomic spectroscopic data [22,23], the radiative lifetime of $He^+(2p)$ is about 100 ps and that of $He^+(2s)$ state is 2 ms. As one can see in Fig. 2, ICD is the dominant decay channel at interatomic distances below 10 Å for all the decaying electronic states. At larger interatomic distances, photon emission starts to be competitive with ICD and it is largely dominant at interatomic distances above 20 Å.

A. Impact of the nuclear dynamics

We showed in Ref. [12] that nuclear dynamics during ICD is essential to describe the electronic decay and has a strong impact on the KER spectra. We give here a detailed analysis of the nuclear dynamics for one given electronic state, namely $^2\Pi_u$:$2p_{x,y}$. The nuclear dynamics on the other electronic states is very similar.

After photoionization of one helium atom in the dimer, the nuclear wave function is a linear combination of nuclear vibrational levels of the decaying electronic state. Due to the large size of the vibrational wave function in the electronic ground state of helium dimer, several vibrational levels are populated. Franck-Condon factors of the vibrational levels as well as of the lowest-lying dissociative states are shown in Fig. 3. As seen in the left panel of the figure, the highest excited level is the most populated. The wave function of this level is extended over a large interatomic distances range and thus has a large overlap with the initial vibrational wave function. We computed the lifetimes of the decaying vibrational states from the imaginary part of their energy. The results for the bound vibrational levels are shown in Table I. As seen in the table, the ICD lifetime varies between 20 fs and 50 ps depending on the vibrational level populated during the photoionization process. These lifetimes are shorter than the radiative lifetime of $He^+(2p)$. This shows that these states decay almost entirely by ICD. In the right panel of Fig. 3, we show the Franck-Condon factors for vibrational states above the dissociation limit. The lowest-lying levels of these discretized continuum are also populated but they decay mainly by emitting a photon (not shown). Since the radiative decay is long, the dimer in these nuclear continuum states dissociates into $He^+(n = 2)$ and He before the excited ion relaxes radiatively. Therefore, no stable He_2^+ dimers are formed. This is in good agreement with the experimental results of T. Havermeier *et al.* which did not detect any stable He_2^+ [11] after photoionization and excitation of helium dimer.

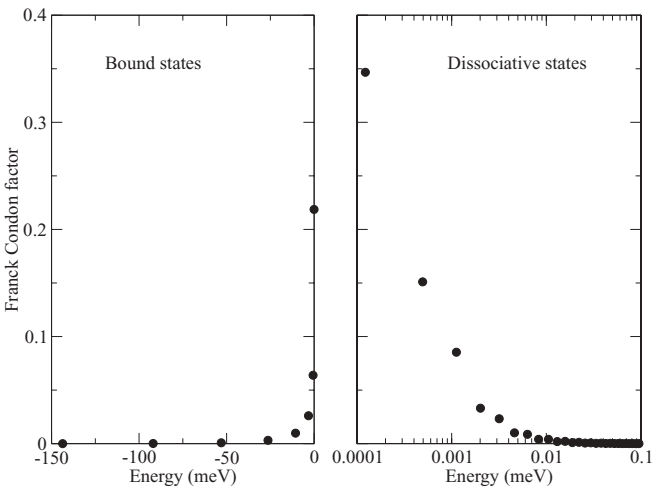

FIG. 3. Franck-Condon factors of the vibrational levels of the $^2\Pi_u$:$2p_{x,y}$ electronic state. The highest excited vibrational level is the most populated level by the photoionization process. Low-lying dissociative levels are populated as well. These levels decay radiatively after dissociation of the dimer.

TABLE I. Lifetime of vibrational states of the different decaying electronic levels using the adiabatic approximation and that obtained by taking the nonadiabatic coupling into account. The vibrational levels of the $^2\Pi_u$:$2p_{x,y}$ and $^2\Pi_g$:$2p_{x,y}$ electronic states have the same lifetime in both representations since no nonadiabatic coupling between them occurs. The potential energy curves of the $^2\Sigma_g^+$:$2s$ and $^2\Sigma_u^+$:$2s$ states support only two vibrational levels in the adiabatic approximation.

	Including nonadiabatic coupling				Adiabatic approximation			
v	$^2\Pi_u$:$2p_{x,y}$	$^2\Pi_g$:$2p_{x,y}$	$^2\Sigma_g^+$:$2p_z$,$2s$	$^2\Sigma_u^+$:$2p_z$,$2s$	$^2\Sigma_g^+$:$2p_z$	$^2\Sigma_g^+$:$2s$	$^2\Sigma_u^+$:$2p_z$	$^2\Sigma_u^+$:$2s$
0	22.00 fs	34.08 fs	30.61 fs	33.49 fs	30.60 fs	–	33.49 fs	–
1	27.15 fs	38.25 fs	37.40 fs	36.44 fs	37.38 fs	–	36.44 fs	–
2	39.27 fs	47.43 fs	51.89 fs	49.00 fs	51.88 fs	–	49.00 fs	–
3	61.22 fs	66.06 fs	81.07 fs	69.58 fs	81.01 fs	–	69.61 fs	–
4	127.44 fs	111.16 fs	147.10 fs	113.76 fs	148.07 fs	–	114.32 fs	–
5	387.04 fs	251.72 fs	377.19 fs	261.05 fs	342.97 fs	–	247.79 fs	–
6	1.81 ps	839.12 fs	1.42 ps	957.02 fs	1.21 ps	–	738.95 fs	–
7	15.57 ps	4.56 ps	1.975 ps	2.64 ps	8.43 ps	–	5.956 ps	–
8	–	53.96 ps	24.69 ps	8.71 ps	–	4.18 ns	–	29.93 ns
9	–	–	44.12 ps	8.78 ps	–	0.80 μs	–	0.17 μs

We investigate now the evolution in time of the KER spectrum for $^2\Pi_u$:$2p_{x,y}$ state decaying to $^1\Sigma_g^+$ final state. The KER spectra for different times after the photoionization-excitation process are shown in Fig. 4. The lower panel of the figure shows the KER spectrum after 10, 50, and 100 fs. We see that after 10 fs, there is a broad peak in the spectrum between 3 and 6 eV. These KER values correspond to interatomic distances between the two atoms of 5 and 2.5 Å, respectively. It demonstrates that just after 10 fs, the system relaxes and the two atoms exchange energy of around 40 eV at distances of up to 5 Å. Note that the maximum of the initial vibrational wave function of the neutral helium dimer is at about 6 Å and the wave function goes to zero very quickly at shorter interatomic distances (see Fig. 1). This explains that even though ICD is faster at shorter distances, the first signals appear at KER values corresponding to rather large distances. At longer times after the photoionization step, the nuclear wave packet moves toward shorter distances due to the attractive potential of the decaying electronic state. After 50 fs, a peak in the KER spectrum around 8 eV appears, corresponding to interatomic distances around 2 Å. It is clear here that time-resolved KER spectrum allows us to follow in time the nuclear wave packet. After 100 fs, the signal around 8 eV becomes the most intense peak. This shows that ICD is much faster at shorter distances as we have seen in Fig. 2 and discussed above. As time proceeds, structures in the KER spectrum become visible. The top panel of Fig. 4 shows the KER spectrum at 200 fs, 1 ps, 2 ps, 10 ps, and 100 ps after the photoionization process. The KER spectrum grows with time and nodal structures in the spectrum become more and more visible. The KER spectra at 10 and 100 ps are almost identical. This shows that the system has completely relaxed after 10 ps. It should be noted that this corresponds to the lifetime of the highest excited vibrational levels as shown in Table I.

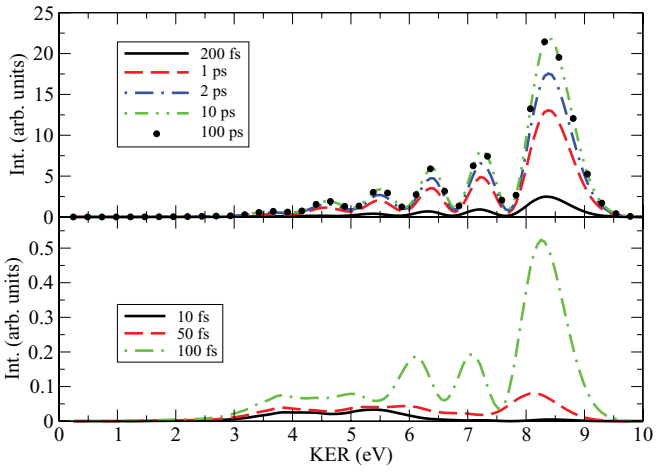

FIG. 4. (Color online) Evolution in time of the KER spectrum for the $^2\Pi_u$:$2p_{x,y}$ electronic state decaying into the $^1\Sigma_g^+$ final state. Time-resolved KER spectra allow us to follow the nuclear wave packet onto the decaying electronic state: at $t = 10$ fs, a broad peak appears between 3 and 6 eV corresponding to $R = 5$ and 2.5 Å, respectively. As time proceeds, the nuclear wave packet moves toward shorter R and distinct peaks arise. The peak at KER = 8.5 eV corresponds to $R = 2$ Å.

The measured total KER spectrum reported in Ref. [11] and in Fig. 5 corresponds to the spectrum after the complete decay of the system. As shown later, the total KER spectrum is the sum of all partial KER spectra computed at time equal infinity. Although not yet achieved for ICD, it is in principle possible to measure time-resolved KER spectra, for instance, by pump-probe experiments as already done for Auger decay [24]. Time-resolved measurements would allow to follow in time the nuclear dynamics on the PEC of the decaying state and would give more insights into the underlying electronic processes.

We show in Fig. 5 the KER spectrum for each ICD channel (i.e., for each pair of decaying electronic states and final states) obtained after that the system has completely decayed. They exhibit structures that, as we showed earlier, are the signature of the nodal structures of the vibrational wave functions involved in the ICD process. In the top panel of Fig. 5, we show the total KER spectrum obtained by summing all partial KER spectra computed at time equal infinity, as well as the total KER spectrum measured by Havermier *et al.* [11]. A good

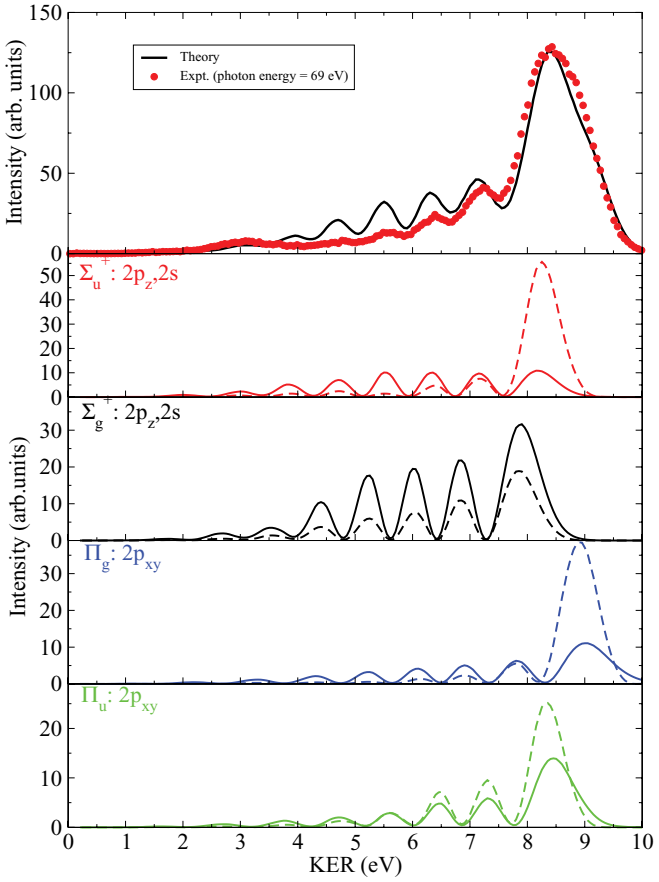

FIG. 5. (Color online) Lower panels: KER distribution of the two He^+ ions after ICD for the different $He^+(n = 2)$-He electronic states decaying into singlet (dashed-line) and triplet (full line) He^+-He^+ states. Top panel: Total KER distribution computed (i.e., sum of all partial KER spectra) and that measured by T. Havermeier *et al.* [11].

agreement between theory and experiment is achieved. The total KER spectrum is discussed in details in Ref. [12]. Small disagreements are visible in the KER range of 4 to 7 eV. From the theoretical side, nonadiabatic effects and the accuracy of the decay rates and of the PEC of the neutral helium dimer could be the main reasons of these disagreements. We discuss them in the following.

B. PEC of the neutral helium dimer

The neutral helium dimer is extremely weakly bound. Computations of the corresponding PEC is thus a delicate issue. It was previously computed by Tang *et al.*, who predicted a mean value of the interatomic distance of around 52 Å. This value is in good agreement with the available experiments [25]. Recently, another group recomputed the PEC [15], taking into account relativistic and quantum electrodynamics effects. From this new PEC, a mean value of the interatomic distance of around 47 Å is obtained. The results shown above and in Ref. [12] were obtained using the PEC from Tang *et al.* We have now also computed the total KER spectrum employing the more recent PEC. Both KER spectra are shown for comparison in Fig. 6. They are very similar over the whole KER range. In fact, the changes in the initial wave function

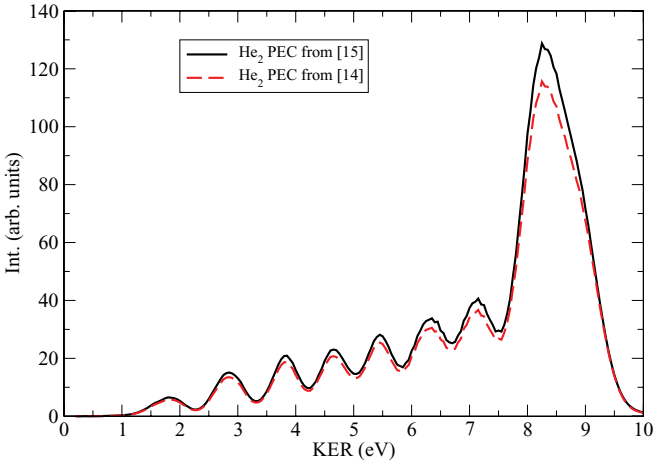

FIG. 6. (Color online) Comparison of the total KER spectrum computed using the ground state PEC of He_2 obtained by Refs. [14,15]. The two KER spectra are similar, except that the intensity of the KER spectrum obtained employing PEC from Ref. [15] is 10% higher. Since the experiment does not determine the absolute intensity of the spectrum, it is not possible here to conclude which PEC is more accurate.

increase the Franck-Condon factors for all vibrational levels by about 10%. These rather moderate changes do not alter much the nuclear dynamics after the photoionization process which is similar in both cases. The absolute values of the total KER spectrum differ, however, by about 10%. Thus, measuring and computing the absolute intensity of the total KER spectrum can be used to identify which PEC of the neutral helium dimer is more accurate. We would like to add that if it will be possible in the future to carry out the experiment by populating only one decaying electronic state or, preferably, one single decaying vibronic level, it would be easier to conclude which PEC is more accurate.

C. Nonadiabatic effects

The PECs of the Σ_g^+:$2p_z$ and Σ_g^+:$2s$ states as well as those of Σ_u^+:$2p_z$ and Σ_u^+:$2s$ states are very close (less than 1 meV) to each other over a wide range of internuclear distances. Consequently, the pair of states with the same symmetry cannot be considered separately and one has to investigate their nonadiabatic couplings. We discuss here the impact of the nonadiabatic effects on the ICD process. Note that the results presented in Fig. 2 and in Ref. [12] were obtained by taking into account these nonadiabatic effects. The nonadiabatic coupling between Σ_g^+:$2p_z$ and Σ_g^+:$2s$ states on one hand and Σ_u^+:$2p_z$ and Σ_u^+:$2s$ states on the other hand were computed explicitly from the respective CI wave functions. Because each electronic state is described by 14 520 Slater determinants, it is numerically demanding to take into account so many determinants to compute the coupling. Therefore, we took the 1000 most contributing determinants (with the biggest CI coefficients) to compute the coupling. Convergence of the coupling with respect to the number of determinants was checked. We used the diabatization method developed by Heil and Dalgarno [26] to calculate diabatic PECs and the coupling between the diabatic states. The adiabatic and

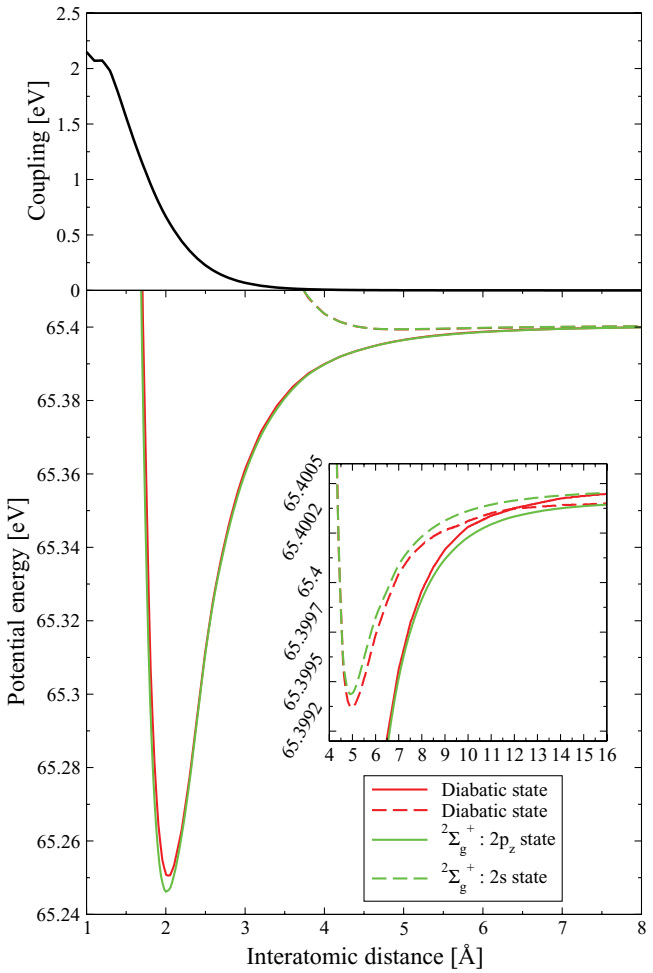

FIG. 7. (Color online) Adiabatic versus diabatic states. Top panel: Coupling between the diabatic states. Lower panel: Diabatic [red (dark gray) lines] and adiabatic [green (light gray) lines] potential energy curves for the Σ_g^+ states. The 1000 most significant determinants (i.e., with the biggest CI coefficients) of the CI wave functions were used to compute the nonadiabatic coupling. The convergence of the coupling with respect to the number of determinants was checked.

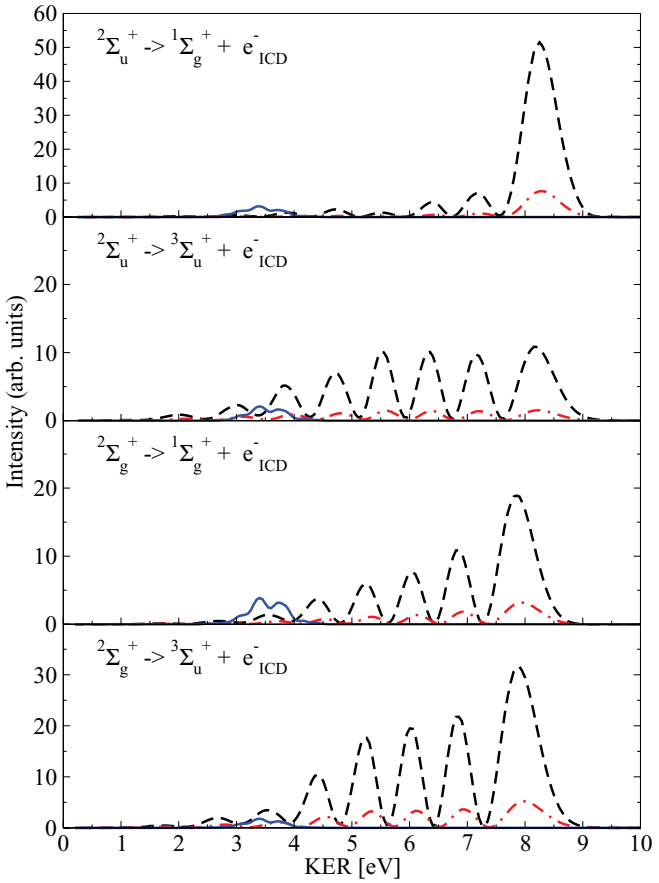

FIG. 8. (Color online) Comparison between the partial KER spectra computed using the adiabatic approximation (dashed-dotted red line and full blue line) and those obtained by taking the nonadiabatic coupling into account (dashed black line) for the different $He^+(n = 2)$-He electronic states of Σ symmetry decaying into singlet and triplet He^+-He^+ states.

diabatic PECs as well as the coupling between the diabatic states are presented in Fig. 7 for the Σ_g^+ states. The findings and conclusions for the Σ_u^+ states are similar. At large interatomic distances, the diabatic and the adiabatic PECs are identical. At shorter interatomic distances, they have a different behavior: the diabatic PECs cross each other at $R = 12$ Å, whereas the adiabatic PECs, which cannot cross due to the noncrossing rule, split up. At even shorter distances, around the minima of the PECs, the diabatic and adiabatic PECs are similar again. The coupling between the diabatic states is negligible at interatomic distances larger than 5 Å and increases at shorter interatomic distances. The KER distributions were calculated using Eqs. (2) and (4) for the *uncoupled* adiabatic states and employing Eq. (5) for the *coupled* diabatic states. In Fig. 8, we show the KER spectra obtained in both representations. The KER spectra for the adiabatic Σ_g^+:$2p_z$ state exhibit a series of peaks between 1 and 10 eV, whereas those for Σ_g^+:$2s$ adiabatic state present a single small peak centered around 3.5 eV. The KER spectra for the coupled diabatic states are similar in appearance to that for the Σ_g^+:$2p_z$ adiabatic state but are about 5 times more intense than the latter over the whole KER range. It is clear that the main effect of the nonadiabatic coupling is to enhance the ICD process. Indeed, as seen in Table I, the Σ_g^+:$2s$ state in the adiabatic representation has a long lifetime and decays mainly radiatively. But because of the nonadiabatic coupling, the lifetime of this state is substantially shortened (e.g., the decay rates of each vibrational states of the Σ_g^+:$2s$ electronic state are 100–20 000 times larger when the nonadiabatic coupling is taken into account) and these states give a larger contribution to the KER spectra.

We show in Fig. 9 the first vibrational state of the Σ_g^+:$2s$ electronic state in the adiabatic approximation and the respective vibronic state computed by taking the nonadiabatic coupling into account. The vibronic wave function is nonzero at interatomic distances between 2 and 4 Å which is an internuclear distance range forbidden in the adiabatic representation. The oscillatory tail of the vibronic wave function at short interatomic distances comes from contributions of vibrational states of the Σ_g^+:$2p_z$ electronic state. This is possible due to the nonadiabatic coupling. The two helium atoms are allowed to come closer and since ICD is dominant

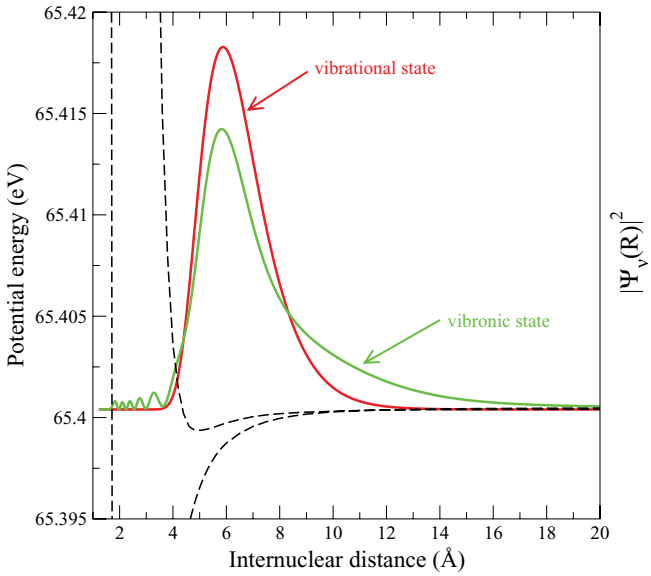

FIG. 9. (Color online) Density of probability associated with the first vibrational state of the Σ_g^+:2*s* electronic state in the adiabatic [red (dark gray) line] approximation and the respective vibronic state [green (light gray) line] computed using the coupled diabatic states, i.e., by including the non-adiabatic coupling. The adiabatic potential energy curves of the Σ_g^+ states are shown as well (dashed black lines).

at short interatomic distances, the Σ_g^+:2*s* electronic state relaxes via ICD instead of by emitting a photon. Moreover, the vibronic states emerging from Σ_g^+:2*s* electronic state are located at rather long interatomic distances and their overlap with the large vibrational wave function of helium dimer in its electronic ground state are significant. Therefore, these states are strongly populated during the photoionization process. This explains why the intensities of the KER spectra are much larger when the nonadiabatic couplings are taken into account.

D. On the impact of the accuracy of the decay rates

The decay rates calculations represent the bottleneck of the present study. The Fano-Green's functions Stieltjes imaging method stands for the currently most complete description of the interatomic decay rates. It is known for being able to produce stable and converged results for the ICD rates ranging over six orders of magnitude or more. Benchmark calculations of atomic Auger and Coster-Kronig decays indicate that typical inaccuracy of the method is to be expected around 10%–15% [16]. Yet, the present problem differs from previously studied cases in that the decaying electronic states are satellite states in the spectrum of the singly ionized helium dimer. This may result in a serious decrease of the quality of their representation since in the present implementation satellite states are treated only within the first order of perturbation theory [13]. Owing to the complexity of the entire method, it is currently impossible to reliably assess the effects of this issue on the resulting decay rates. In order to deal with this uncertainty we investigate here the effects on the total KER spectrum obtained by changing the magnitude of the decay rates.

In Fig. 10, we show the KER spectrum obtained using the *ab initio* data taken from Ref. [13], as presented in Fig. 1,

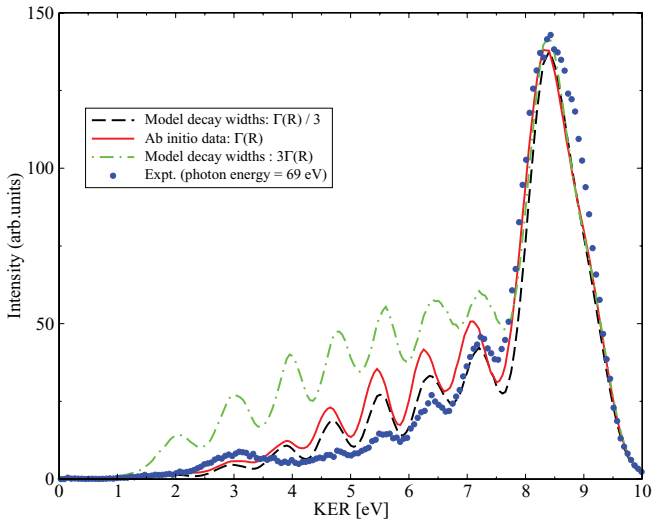

FIG. 10. (Color online) Total KER spectra computed with decay rates of different magnitude. The spectra are compared to experimental spectrum (blue circles). The small discrepancies between theory and experiment cannot be attributed solely to a possible inaccuracy of the decay rates.

and two additional KER spectra obtained using the decay rates (both total and partial) either divided or multiplied by 3. The factor of 3 was chosen to safely cover any potential uncertainties in the decay rates calculations. For comparison, the measured KER spectrum is also shown in Fig. 10. All KER distributions were scaled so the highest peak has the same intensity as in the experiment. We observe that with increasing decay rates the low KER is enhanced, whereas decreasing the decay rates makes the intensity of the low KER peaks smaller. This behavior can be explained using the following arguments: at large interatomic distances, the ICD efficiency is suppressed by the radiative decay. Increasing the ICD rates reduces the effect of radiative decay. Hence, the low KER, which corresponds to ICD at large interatomic distances, is enhanced relative to high KER. For the same reason, decreasing the decay rates makes the photon emission a more effective decay channel.

As can be seen in Fig. 10, the agreement between theory and experiment is best for the reduced decay rates. However, the difference from the results obtained using the *ab initio* data is rather small. On the other hand, increasing the ICD rates by the factor of 3 clearly deteriorates the agreement. Still, some discrepancies for low KER exist in all cases. We conclude that a possible inaccuracy of the decay rates cannot be the only reason for the small differences between the theory and experiment.

IV. CONCLUSIONS

We reported a detailed analysis of the nuclear dynamics during the interatomic electronic decay in the giant helium dimer. The effects of the two different potential energy curves available for the electronic ground state were studied. The total KER spectrum is rather insensitive to the small disagreements between the two curves. We also investigated the effects of the nonadiabatic coupling on the KER spectra. The adiabatic

approximation fails to describe correctly the ICD process, because of nonadiabatic effects between the Σ_g^+:$2p_z$ and Σ_g^+:$2s$ states and between the Σ_u^+:$2p_z$ and Σ_u^+:$2s$ states. We showed that the ICD process is significantly enhanced when the nonadiabatic coupling is taken into account. Finally, we demonstrated that the rather small differences between the computed and the measured total KER spectrum cannot be explained solely by a possible inaccuracy of the ICD rates. We should mention that recoil effects [27,28] were not taken into account and might change the KER spectra.

ACKNOWLEDGMENTS

We thank R. Dörner, T. Havermeier, and T. Jahnke for fruitful discussions. Financial support by the European Research Council (ERC Advanced Investigator Grant No. 227597), the Alexander von Humboldt foundation, the Czech Science Foundation (Grant No. GAČR 202/09/0786), the Japanese Society for the Promotion of Science, and the Deutsche Forschungsgemeinschaft is acknowledged by L.S.C., N.S., P.K., S.S., and N.V.K., respectively.

[1] L. S. Cederbaum, J. Zobeley, and F. Tarantelli, Phys. Rev. Lett. **79**, 4778 (1997).
[2] S. Marburger, O. Kugeler, U. Hergenhahn, and T. Möller, Phys. Rev. Lett. **90**, 203401 (2003).
[3] T. Jahnke *et al.*, Phys. Rev. Lett. **93**, 163401 (2004).
[4] S. Barth, S. Joshi, S. Marburger, V. Ulrich, A. Lindblad, G. Öhrwall, O. Björneholm, and U. Hergenhahn, J. Chem. Phys. **122**, 241102 (2005).
[5] T. Aoto, K. Ito, Y. Hikosaka, E. Shigemasa, F. Penent, and P. Lablanquie, Phys. Rev. Lett. **97**, 243401 (2006).
[6] K. Kreidi *et al.*, Phys. Rev. A **78**, 043422 (2008).
[7] E. F. Aziz, N. Ottosson, M. Faubel, I. V. Hertel, and B. Winter, Nature (London) **455**, 89 (2008).
[8] T. Jahnke *et al.*, Nat. Phys. **6**, 139 (2010).
[9] M. Mucke, M. Braune, S. Barth, M. Förstel, T. Lischke, V. Volker, T. Arion, U. Becker, A. Bradshaw, and U. Hergenhahn, Nat. Phys. **6**, 143 (2010).
[10] T. Jahnke *et al.*, Phys. Rev. Lett. **99**, 153401 (2007).
[11] T. Havermeier *et al.*, Phys. Rev. Lett. **104**, 133401 (2010).
[12] N. Sisourat, N. V. Kryzhevoi, P. Kolorenč, T. Jahnke, S. Scheit, and L. S. Cederbaum, Nat. Phys. **6**, 508 (2010).
[13] P. Kolorenč, N. V. Kryzhevoi, N. Sisourat, and L. S. Cederbaum, Phys. Rev. A **82**, 013422 (2010).
[14] K. T. Tang, J. P. Toennies, and C. L. Yiu, Phys. Rev. Lett. **74**, 1546 (1995).
[15] M. Przybytek, W. Cencek, J. Komasa, G. Łach, B. Jeziorski, and K. Szalewicz, Phys. Rev. Lett. **104**, 183003 (2010).
[16] V. Averbukh and L. S. Cederbaum, J. Chem. Phys. **123**, 204107 (2005).
[17] V. Averbukh and L. S. Cederbaum, J. Chem. Phys. **125**, 094107 (2006).
[18] N. Moiseyev, S. Scheit, and L. S. Cederbaum, J. Chem. Phys. **121**, 722 (2004).
[19] L. S. Cederbaum and W. Domcke, J. Phys. B **14**, 4665 (1981).
[20] E. Pahl, H.-D. Meyer, L. S. Cederbaum, D. Minelli, and F. Tarantelli, J. Chem. Phys. **105**, 9175 (1996).
[21] W. H. Press, B. P. Flannery, S. A. Teukolsky, and W. T. Vetterling, *Numerical Recipes*, 2nd ed. (Cambridge University Press, Cambridge, 1992).
[22] G. W. F. Drake, J. Kwela, and A. van Wijngaarden, Phys. Rev. A **46**, 113 (1992).
[23] M. H. Prior, Phys. Rev. Lett. **29**, 611 (1972).
[24] M. Drescher *et al.*, Nature (London) **419**, 803 (2002).
[25] R. E. Grisenti, W. Schöllkopf, J. P. Toennies, G. C. Hegerfeldt, T. Köhler, and M. Stoll, Phys. Rev. Lett. **85**, 2284 (2000).
[26] T. G. Heil and A. Dalgarno, J. Phys. B **12**, L557 (1979).
[27] W. Domcke and L. S. Cederbaum, J. Electron Spectrosc. Relat. Phenom. **13**, 161 (1978).
[28] K. Kreidi *et al.*, Phys. Rev. Lett. **103**, 033001 (2009).